Protein Structure and Folding:

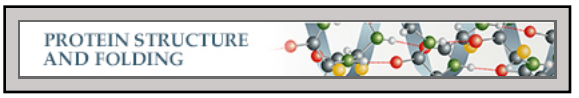

Does the Cytotoxic Effect of Transient Amyloid Oligomers from Common Equine Lysozyme *in Vitro* Imply Innate Amyloid Toxicity?

Mantas Malisauskas, Johan Ostman, Adas Darinskas, Vladimir Zamotin, Evaldas Liutkevicius, Erik Lundgren and Ludmilla A. Morozova-Roche

J. Biol. Chem. 2005, 280:6269-6275.
doi: 10.1074/jbc.M407273200 originally published online December 1, 2004

Access the most updated version of this article at doi: 10.1074/jbc.M407273200

Find articles, minireviews, Reflections and Classics on similar topics on the JBC Affinity Sites.

Alerts:
- When this article is cited
- When a correction for this article is posted

Click here to choose from all of JBC's e-mail alerts

This article cites 32 references, 9 of which can be accessed free at
http://www.jbc.org/content/280/8/6269.full.html#ref-list-1

Downloaded from http://www.jbc.org/ by guest on January 16, 2014

THE JOURNAL OF BIOLOGICAL CHEMISTRY
Vol. 280, No. 8, Issue of February 25, pp. 6269–6275, 2005
Printed in U.S.A.
© 2005 by The American Society for Biochemistry and Molecular Biology, Inc.

Does the Cytotoxic Effect of Transient Amyloid Oligomers from Common Equine Lysozyme *in Vitro* Imply Innate Amyloid Toxicity?*

Received for publication, June 29, 2004, and in revised form, November 30, 2004
Published, JBC Papers in Press, December 1, 2004, DOI 10.1074/jbc.M407273200

Mantas Malisauskas‡§, Johan Ostman¶, Adas Darinskas‖, Vladimir Zamotin‡, Evaldas Liutkevicius‖, Erik Lundgren¶, and Ludmilla A. Morozova-Roche‡

From the Departments of ‡Medical Biochemistry and Biophysics and ¶Cell and Molecular Biology, Umeå University, Umeå 90187, Sweden and ‖Laboratory of Pharmacology, Institute of Immunology, Vilnius University, Vilnius 08409, Lithuania

In amyloid diseases, it is not evident which protein aggregates induce cell death via specific molecular mechanisms and which cause damage because of their mass accumulation and mechanical properties. We showed that equine lysozyme assembles into soluble amyloid oligomers and protofilaments at pH 2.0 and 4.5, 57 °C. They bind thioflavin-T and Congo red similar to common amyloid structures, and their morphology was monitored by atomic force microscopy. Molecular volume evaluation from microscopic measurements allowed us to identify distinct types of oligomers, ranging from tetramer to octamer and 20-mer. Monomeric lysozyme and protofilaments are not cytotoxic, whereas the oligomers induce cell death in primary neuronal cells, primary fibroblasts, and the neuroblastoma IMR-32 cell line. Cytotoxicity was accessed by ethidium bromide staining, MTT reduction, and TUNEL assays. Primary cultures were more susceptible to the toxic effect induced by soluble amyloid oligomers than the neuroblastoma cell line. The cytotoxicity correlates with the size of oligomers; the sample incubated at pH 4.5 and containing larger oligomers, including 20-mer, appears to be more cytotoxic than the lysozyme sample kept at pH 2.0, in which only tetramers and octamers were found. Soluble amyloid oligomers may assemble into rings; however, there was no correlation between the quantity of rings in the sample and its toxicity. The cytotoxicity of transient oligomeric species of the ubiquitous protein lysozyme indicates that this is an intrinsic feature of protein amyloid aggregation, and therefore soluble amyloid oligomers can be used as a primary therapeutic target and marker of amyloid disease.

The molecular basis of the pathogenicity of amyloid aggregates is a central theme in understanding the causes of a wide range of amyloid-related diseases, including Alzheimer's, Parkinson's, prion diseases, type II diabetes, and familial amyloidotic polyneuropathy (1–4). There is a striking difference between the amounts of amyloid depositions in various types of amyloid disorders. In systemic lysozyme amyloidosis, for example, the deposits can grow to kilogram quantities in the liver (5, 6). In neurodegenerative diseases, by contrast, there is no clear correlation between the amount of amyloid deposition and the clinical severity of disease. Significant cognitive impairment of Alzheimer's patients was observed without noticeable amyloid deposits in the brain, although the level of readily soluble amyloid oligomeric assemblies in the Alzheimer's brain was found to be greatly elevated (7, 8).

The evidence is accumulating that prefibrillar aggregates are cytotoxic both *in vivo* and *in vitro* (4, 8, 9), although this question is still open to debate. Moreover, aggregates of the proteins, which are not related to clinical amyloidoses, such as human α-lactalbumin (10), SH3 domain, or HypF-N protein, have also been found to be cytotoxic, which implies a common mechanism for cytotoxicity of misfolded proteins (11). By contrast, it has been shown that the mature amyloid fibrils of amyloid β peptide and transthyretin are not toxic (4, 12). It is still not evident, however, which particular amyloid structures induce cell death by specific molecular mechanisms and which play the role of "inert" material and cause disease due to their quantity or mechanical properties.

In our research, we addressed this problem by subjecting well defined oligomeric intermediates of equine lysozyme (EL)[1] to the toxicity assays on different cell types. EL belongs to an extended family of structurally related proteins, chicken-type lysozymes, and α-lactalbumins. It possesses a calcium-binding site similar to α-lactalbumins and a bacteriolytic enzymatic activity like conventional lysozymes. It combines also the structural and folding properties of both subfamilies and is viewed as an evolutionary bridge between them (13–15).

In the 1990s, it was found that amyloidogenic mutants of human lysozyme are involved in systemic amyloidosis (6), whereas wild-type human lysozyme also is able to form amyloid fibrils *in vitro* (16). Oligomers of human α-lactalbumin (HAMLET) appeared to be toxic to immature and tumor cells (11). Recently, we have demonstrated that, in contrast to lysozymes and α-lactalbumins (16, 17), EL forms morphologically very distinct linear and annular protofilaments, depending on calcium ion concentrations and pH (18). In the present study, the soluble amyloid oligomers of EL were produced under fibrillation conditions prior to development of the filamentous structures, and their toxicity was assessed in comparison with the monomeric and fibrillar species. This analysis revealed that toxicity depends on the size of soluble amyloid oligomers.

* This work was supported by the Swedish Medical Research Council. The costs of publication of this article were defrayed in part by the payment of page charges. This article must therefore be hereby marked "*advertisement*" in accordance with 18 U.S.C. Section 1734 solely to indicate this fact.

§ Supported by the Lilly and Sven Lawskis Foundation.

** Supported by the Swedish Medical Research Council. To whom correspondence should be addressed: Dept. of Medical Biochemistry and Biophysics, Umeå University, Umeå 90187, Sweden. Tel.: 46-90-7865283; Fax: 46-90-7869795; E-mail: Ludmilla.Morozova-Roche@chem.umu.se.

[1] The abbreviations used are: EL, equine lysozyme; AFM, atomic force microscopy; ThT, thioflavin-T; EtBr, ethidium bromide; MTT, 3-(4,5-dimethylthiazol-2-yl)-2,5-diphenyltetrazolium bromide; TUNEL, transferase-mediated dUTP nick-end-labeling; SPIP, Scanning Probe Image Processor; SH, Src homology.

Downloaded from http://www.jbc.org/ by guest on January 16, 2014

EXPERIMENTAL PROCEDURES

Protein Samples—Holo-EL was purified from horse milk as described previously (19). Protein concentration was determined by absorbance measurements on a Beckman UV-VIS spectrophotometer at 280 nm using an extinction coefficient, $E_{1\%} = 23.5$. To produce amyloid structures, EL was incubated at a 20 mg/ml (1.36 mM) concentration in 20 mM glycine (pH 2.0) or 10 mM sodium acetate (pH 4.5) buffers with 0.2% sodium azide at 57 °C, as described previously (18).

Amyloid Assays—Thioflavin-T (ThT) binding assay was performed as described previously (16). Fluorescence of ThT was measured on a FluoroMax-2 spectrofluorometer (JOBIN YVON/PSEX Instruments) using excitation at 440 nm, emission between 450–550 nm, and setting the excitation and emission slits at 5 nm.

Congo red binding assay was performed as described by Klunk *et al.* (20). Absorbance spectra of the reaction solution were collected together with negative controls containing dye and protein separately, subtracting from the former the signals associated with the absorption of the dye and the scattering contribution from the fibrils.

Atomic Force Microscopy (AFM)—AFM measurements were performed on a PicoPlus AFM (Molecular Imaging) in a tapping mode using a 100-μm scanner. Acoustically and magnetically driven cantilevers were used for imaging under both ambient and liquid conditions. Both cantilevers have etched silicon probes of the TESP model with diameters of 10 nm and less (Digital Instruments). In the acoustic mode, we applied a resonance frequency in the 170–190 kHz range, a scan rate of 1 Hz, and a resolution of 512 × 512 pixels. In magnetic mode, the cantilevers operated at a resonance frequency of ~25 kHz, a scan rate of 1–2 Hz and a resolution of 256 × 256 or 512 × 512 pixels. Height, amplitude, and phase data were collected simultaneously. Images were flattened and plane adjusted. The scanning of samples was performed in trace and retrace to avoid the scan artifacts. The scanner was calibrated by measuring atomic steps on a highly orientated pyrolytic graphite in the *z*-axis and using a standard 1-μm calibration grid (Molecular Imaging) in the *xy* plane.

For ambient imaging, amyloid samples (200 μg/ml) were deposited on the surface of freshly cleaved mica (GoodFellow) for 5 s, washed three times with 250 μl of MilliQ water, and dried at room temperature. For imaging in fluid, the samples were diluted to 50–80 μg/ml, placed on the mica for 10 min, washed three times with 200 μl of buffer solution, and a final 300-μl solution was added to the open liquid cell. The short adsorption time of the amyloid species on the mica substrate (compared with hours and days of the incubation period) and the high dilution of the samples ensured that aggregation was not triggered by the mica surface. Graphite was used as a substrate in control measurements. Topographical images of soluble amyloid oligomers and fibrils were essentially the same under all conditions.

Measuring Molecular Dimensions—The dimensions of protein species were measured in multiple cross-sections of the same particle in AFM height images using PicoPlus software (Molecular Imaging). The distribution of the *z*-heights of particles was also evaluated by applying the grain analysis module of Scanning Probe Image Processor (SPIP) software (Image Metrology). In the latter, the heights of all species above the threshold surface set at the noise level were measured. To build an average height distribution, 3–4 areas on the mica surface of 1 × 1-μm size, with 1000–4000 particles in each, were subjected to the SPIP grain analysis in each sample; the experiments were repeated three times. Because of adhesion forces, the molecular species were spread on the mica surface, giving larger lateral measurements compared with vertical dimensions. Generally, an AFM tip also contributes to the broadening effect because of its specific geometry. To evaluate the tip geometry and the accuracy of our measurements, we used the tip deconvolution module of the SPIP software and performed measurements on the reference samples, such as carbon nanotubes with ~1-nm diameters and spherical latex particles with ~1.5-nm diameters. Processing images with the SPIP tip deconvolution module indicated that the shape of the tip did not produce topological artifacts. Measurements of the reference samples confirmed the previous conclusions (21, 22) that the diameter at the half-maximal height of the individual protein particle treated as a spherical cap sufficiently compensates for the AFM-induced broadening of the *xy* dimensions. The volume of each particle was derived from Equation 1,

$$V_{\mathrm{AFM}} = (\pi h/6)(3r^2 + h^2) \qquad \text{(Eq. 1)}$$

where h is the particle height, and r is the radius at half-height (21).

The molecular volume of monomeric EL was estimated using,

$$V_m = (M_o/N_o)(V_1 + dV_2) \qquad \text{(Eq. 2)}$$

where M_o is the protein molecular weight, N_o is Avogadro's number, d is the extent of protein hydration (0.4 mol H_2O/mol protein), and V_1 and V_2 are the partial specific volumes of protein (0.74 $cm^3\ g^{-1}$) and water (1 $cm^3\ g^{-1}$) molecules, respectively (21). The number of EL monomers in oligomeric species was determined by the following ratio.

$$n = V_{\mathrm{AFM}}/V_m \qquad \text{(Eq. 3)}$$

Cell Cultures—Primary neural cell cultures, containing both neurons and glial cells, and primary mouse embryonic fibroblasts were isolated from 9–12.5 gestation day embryos BALB/c mice, according to the procedure described previously (23, 24). The cells were cultivated as monolayers in Dulbecco's modified Eagle's medium with 1000 mg/liter D-glucose, 110 mg/liter sodium pyruvate, heat-inactivated 10% fetal calf serum, 2 mM L-glutamine, 100 units/ml penicillin/streptomycin (Biological Industries) in 5% CO_2 at 37 °C. The medium was changed everyday.

IMR-32 cells were grown in Dulbecco's modified Eagle's medium supplemented with 20 mM Hepes, 6% fetal bovine serum, 2.4 mM L-glutamate, and 1% PEST in a humidified incubator containing 5% CO_2 and at 37 °C.

The cell viability was assessed after 48 h of incubation with the amyloid structures, as it has been shown previously that the cell metabolic response to added compounds requires hours or days (4, 11, 25, 26). In all cytotoxicity assays, the control measurements were performed after 24 h of incubation with amyloid, and the cell viability was decreased; however the effect was less pronounced than after 48 h.

Cell Staining with Ethidium Bromide (EtBr)—Three days after isolation, the primary cells were confluent. They were diluted three times after treatment with 0.05% trypsin and 0.53 mM EDTA (Invitrogen). Both primary cell cultures and IMR-32 cells were seeded into the cell culture plates (96-well; BD Biosciences) with ~10,000 cells/well in 200 μl of medium. At confluence after 24 h, the medium was changed, and aliquots of EL containing amyloid structures were added to a final concentration of 5–50 μM. In the control experiments, the cells were incubated in the presence of 30 μM amyloid incubation buffer or with 15 μM freshly dissolved monomeric EL.

The cells were incubated in the presence of EL amyloid samples for 48 h and then detached as described above and suspended in the medium. 500-μl aliquots of the cell suspensions in primary mouse embryonic fibroblast medium were stained with 5 μl of 20 mg/ml EtBr for 10 min at 4 °C. Cell viability was estimated using a fluorescence-activated cell sorter (FACS) caliber flow cytometer (Bd Biosciences) according to the procedure described in Ref. 27. The viability was estimated by counting 10,000 events using the Cell Quest program (FACS caliber manual).

Inhibition of MTT Reduction—IMR-32 cells were plated at a density of 10,000 cells/well in 96-well plates. The aliquots of EL amyloid were added to the wells (100 μl) at various final EL concentrations (see Fig. 5), and the cells were incubated for 48 h. 10 μl of 3-(4,5-dimethylthiazol-2-yl)-2,5-diphenyltetrazolium bromide (MTT) labeling reagent was added to each well, and the samples were incubated for a further 4 h. 100 μl of solubilization mixture (10% SDS, 0.01 M HCl) were added to each well, and the samples were incubated overnight. Absorbance of blue formazan at 570 nm was measured with a plate reader (28).

Labeling of Free DNA Ends—IMR-32 cells were cultured in 48-well plates (Nunclon). EL amyloid aliquots were added to the final concentration of 14 and 64 μM, and the slides were further incubated for 48 h. DNA fragmentation was detected by a transferase-mediated dUTP nick-end-labeling (TUNEL) method using a fluorescent staining kit according to the manufacturer's instructions (Roche Diagnostics). Similar aliquots of the incubation buffers (pH 2.0 and 4.5) were added to IMR-32 cells in control experiments. Stained cells were analyzed by flow cytometry as described above.

RESULTS

Structural Characterization of EL Fibrillation—The kinetics of EL self-assembly was monitored using ThT fluorescence assay (Fig.1), which serves as a marker for amyloid (17). Protein aliquots were diluted into a buffer containing ThT after differing periods of incubation. Both samples of EL, incubated at pH 2.0 and 4.5 at 57 °C, were characterized by short lag phases of 3 and 12–14 h, respectively, which correspond to the initiation of nucleation (29). This was followed by an increase of fluorescence intensity reaching a plateau level with 10- and 7.5-fold increases of ThT dye fluorescence bound to EL amyloid incubated for ~120 and ~200 h at pH 2.0 and pH 4.5, respectively (Fig. 1).

Downloaded from http://www.jbc.org/ by guest on January 16, 2014

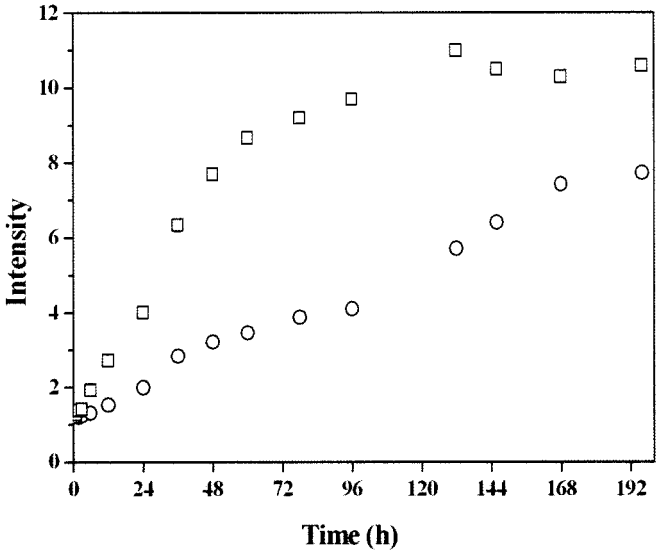

FIG. 1. **Kinetics of EL amyloid formation monitored by ThT fluorescence.** EL was incubated at 20 mg/ml in 10 mM sodium acetate, pH 4.5 (○), and 20 mM glycine, pH 2.0 (□), 57 °C as described under "Experimental Procedures."

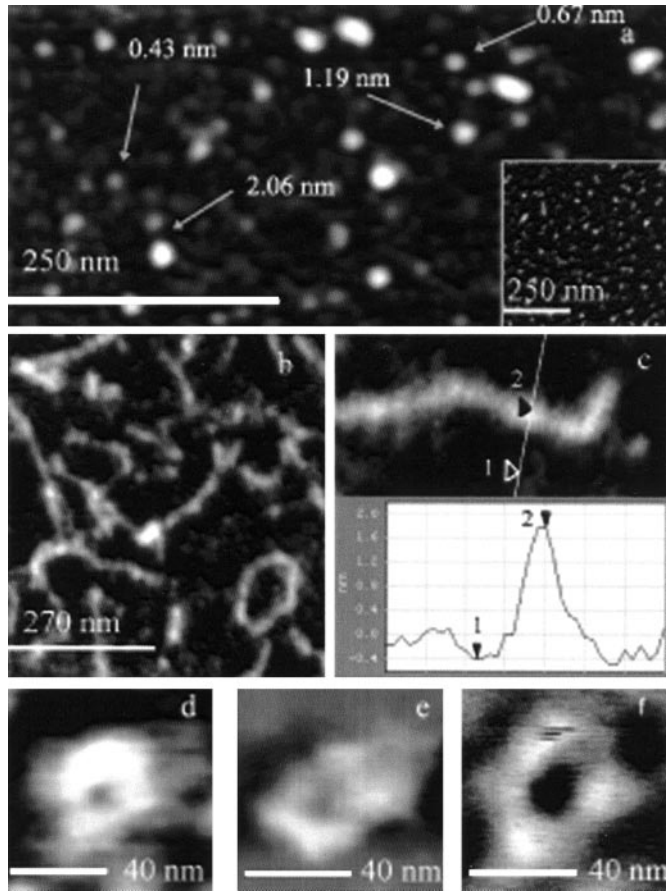

FIG. 2. **Amyloid structures of EL observed by AFM.** *a*, height image of round-shaped oligomers, 72 h of incubation at pH 4.5 and 57 °C. *z*-scale is 7 nm. The same soluble amyloid oligomers imaged after transferring into serum-free culture medium (*inset*). *b*, protofilaments of ~2 nm height, 24 days of incubation at pH 4.5 and 57 °C. *z*-scale is 10 nm. *c*, height image and cross-section of a typical protofilament, demonstrating that its *z*-height is ~2 nm. *d–f*, representative images of annular protofibrils formed after 72 h of incubation at pH 4.5. The species were transferred to serum-free culture medium and imaged in a liquid cell on mica surface (*d*). The pH 4.5 samples were dried in air using graphite (*e*) or mica (*f*) substrates.

EL-aggregated structures were analyzed by AFM. Representative images of EL species are shown in Fig. 2, and their height distribution histograms are presented in Fig. 3. Protein molecules from freshly prepared EL samples adsorbed on the mica surface, which was manifested in a narrow log-normal distribution of *z*-heights with a mean value of 0.4 nm in both cases of pH 4.5 and pH 2.0 (Fig. 3, *a* and *b*). The molecular volumes of these species were evaluated by Equation 1 using their *z*-heights and diameters at half-height, determined by both the grain analysis SPIP software and by multiple cross-section measurements of individual particles. The results are presented in Table I. Both methods gave a good agreement with the calculated volume of EL monomer using Equation 2.

During the growth phase (Fig. 1), the larger round-shaped oligomers were formed in the samples (Fig. 2*a*) characterized by broader distributions of *z*-heights (Fig. 3, *c* and *d*). They gave rise to elongated linear and annular (Fig. 2, *d–f*) protofibrils with a "bead-on-string" morphology. Subsequently the protofilaments with an ~2-nm *z*-height emerged in the samples (Fig. 2, *b* and *c*); the cross-section of a typical protofilament is presented in Fig. 2*c*. The protofilaments were rather short, 30–300 nm in length, and there were both straight and curved sections, whereas some of them were locked into circular structures (Fig. 2*b*). Similar protofilaments were observed previously at pH 4.5 and 57 °C in the presence of 10 mM $CaCl_2$ (18).

After incubation periods of 72 h (pH 4.5) and 24 h (pH 2.0), respectively, both EL samples displayed the same increase in ThT fluorescence and were characterized by the formation of round-shaped oligomers, whereas the protofilaments have not yet been observed. These samples were subjected further to the cytotoxicity assays to compare the effect induced by monomeric, oligomeric, and fibrillar species of EL. The *z*-height histograms of the species produced at these time points were characterized by a decrease of the main peak concomitantly with the appearance of a pronounced right-hand shoulder corresponding to progressive enlargement of oligomers. In the pH 4.5 sample (Fig. 3*c*), a second peak centered at the *z*-height of ~2.1 nm became apparent. The fraction of oligomers with a characteristic *z*-height of ~0.7 nm was determined in both samples at pH 4.5 and 2.0 by subtracting from the histograms at given time points those of freshly dissolved EL (Fig. 3, *e* and *f*). In addition, in the sample incubated at pH 4.5 compared with the sample at pH 2.0, there is a fraction with a *z*-height of ~1.1 (Fig. 3*g*), identified by the difference between the corresponding distributions shown in Fig. 3, *c* and *d*. The control experiments, with a significantly smaller number of particles were carried out using manual cross-section analysis (Table I) to confirm the values obtained from larger screenings by the SPIP grain analysis module (Fig. 3). The volumes of oligomers were calculated by Equation 1 using the linear parameters of oligomers determined in both types of measurements. The stoichiometry of oligomers was calculated using Equation 3 and presented in Table I. Both approaches gave consistent results. The distribution of oligomers in the pH 4.5 sample (Fig. 3*c*) was well fit by a sum of log-normal functions with the means of *z*-height equal to ~0.4, ~0.7, ~1.1, and ~2.1 nm ($\chi^2 = 0.002$) (Fig. 3*h*), although the best fit of the distribution of the pH 2.0 sample was achieved using only two log-normal functions with the means of 0.4 and 0.7 nm ($\chi^2 = 0.005$).

The soluble amyloid oligomers described above (Fig. 2*a*) were characterized by a 2–3-nm long wavelength shift of Congo red spectra compared with a 5–6-nm shift caused by the fibrillar structures formed subsequently. Apart from single round-shaped oligomers in both samples, we also observed characteristic annular protofibrils with 4- or 5-fold symmetry (Fig. 2, *d–f*). They consisted of segments in which *z*-heights and molec-

Downloaded from http://www.jbc.org/ by guest on January 16, 2014

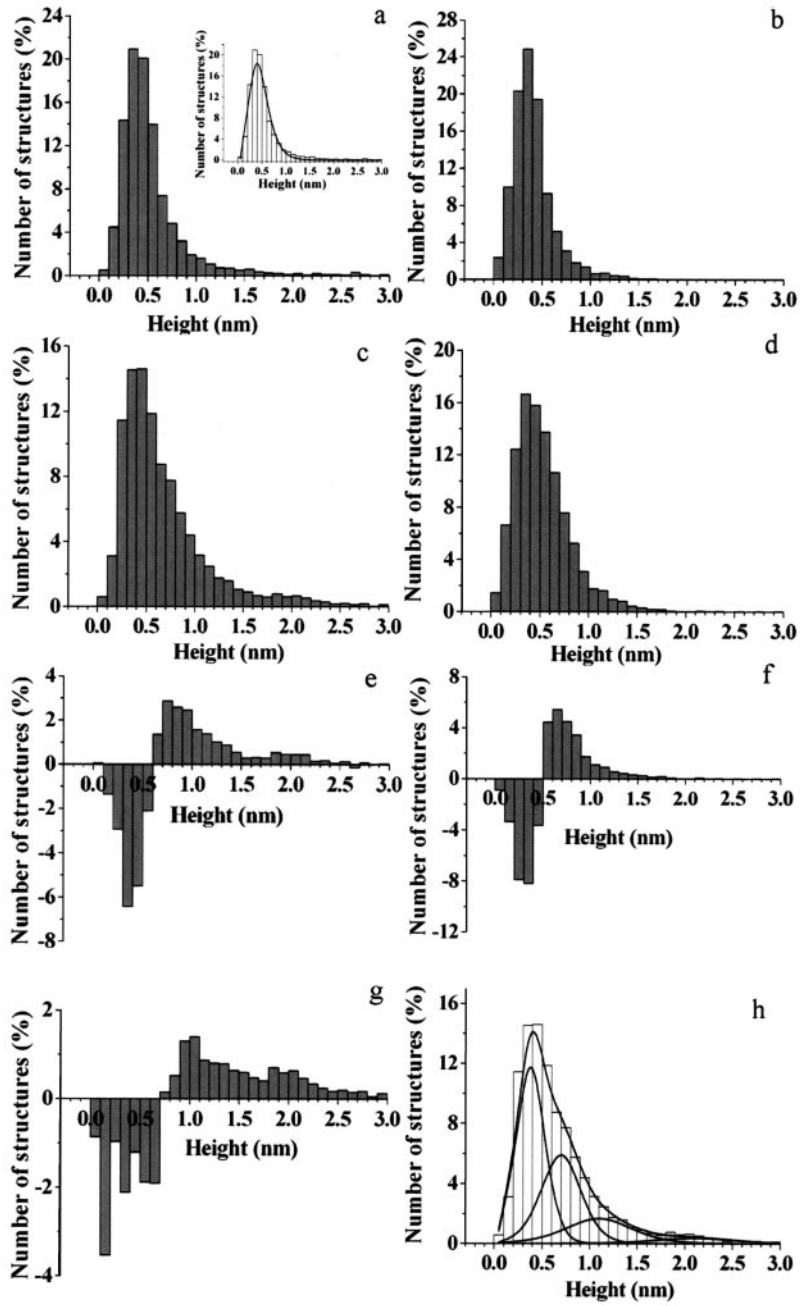

FIG. 3. **Molecular dimensions of EL determined by AFM.** In each protein sample, 3–4 areas of 1 × 1-μm size, with 1000–4000 particles in each area, were subjected to SPIP software grain analysis. The distribution of *z*-heights in the freshly prepared EL samples at pH 4.5 (*a*) and pH 2.0 (*b*) immediately after protein dissolving and after 72 h of incubation at pH 4.5 and 57 °C (*c*) and after 24 h at pH 2.0 and 57 °C (*d*) are shown. The histograms showing the difference between the population of oligomers in the samples *c*−*a* (*e*), *d*−*b* (*f*), and *d*−*c* (*g*) are presented here. The formation of larger species manifested by the appearance of additional maxima with larger *z*-height values. The data were fit to log-normal functions, as shown in the *inset* to *panel a* for the freshly dissolved EL and in *panel h* for the oligomers formed at pH 4.5 and 57 °C after 72 h. To compare the samples, all distributions were normalized to the total number of particles in the scanned field.

TABLE I

Molecular dimensions of EL-soluble amyloid oligomers determined by AFM

The *z*-height and diameter were determined using multiple cross-section analysis; the volume and stoichiometry were calculated using equations 1–3.

Structures	*n*	*h*	Diameter	V_m	No. of monomers	No. of monomers[a]
		nm	*nm*	nm^3		
0.4	9	0.39 ± 0.06	15.7 ± 2.42	38.3 ± 11.6	1 ± 0.5	1 ± 0.5
0.7	8	0.70 ± 0.14	20.96 ± 0.8	122.5 ± 9.4	4 ± 0.5	5 ± 2
1.1	10	1.05 ± 0.114	22.33 ± 1.46	207.9 ± 26.8	8 ± 1	8 ± 3
2.1	8	2.03 ± 0.224	27.85 ± 2.83	584.3 ± 119.0	21 ± 4	25 ± 7

[a] The stoichiometry of oligomers were derived from AFM data using the SPIP grain analysis module.

ular volumes were similar to the dimensions of the individual round-shaped species with *z*-heights of 0.7–1.2 nm present in the same samples (Fig. 2*a*).

The control AFM imaging of the amyloid structures was performed immediately after their transfer from the incubation buffers to serum-free culture medium and in a 48-h incubation in serum-free culture medium at 37 °C. Under these conditions, the morphology and the cross-sectional dimensions of the oligomers, protofibrils, and protofilaments did not change, as shown in the representative images in Fig. 2*a*, *inset*, and Fig. 2, *d–f*). To confirm the stability of the oligomeric structures in the physiological solutions, population analysis using the SPIP software was also performed and compared with the manual measurements in the cross-sections. Immediately after trans-

Downloaded from http://www.jbc.org/ by guest on January 16, 2014

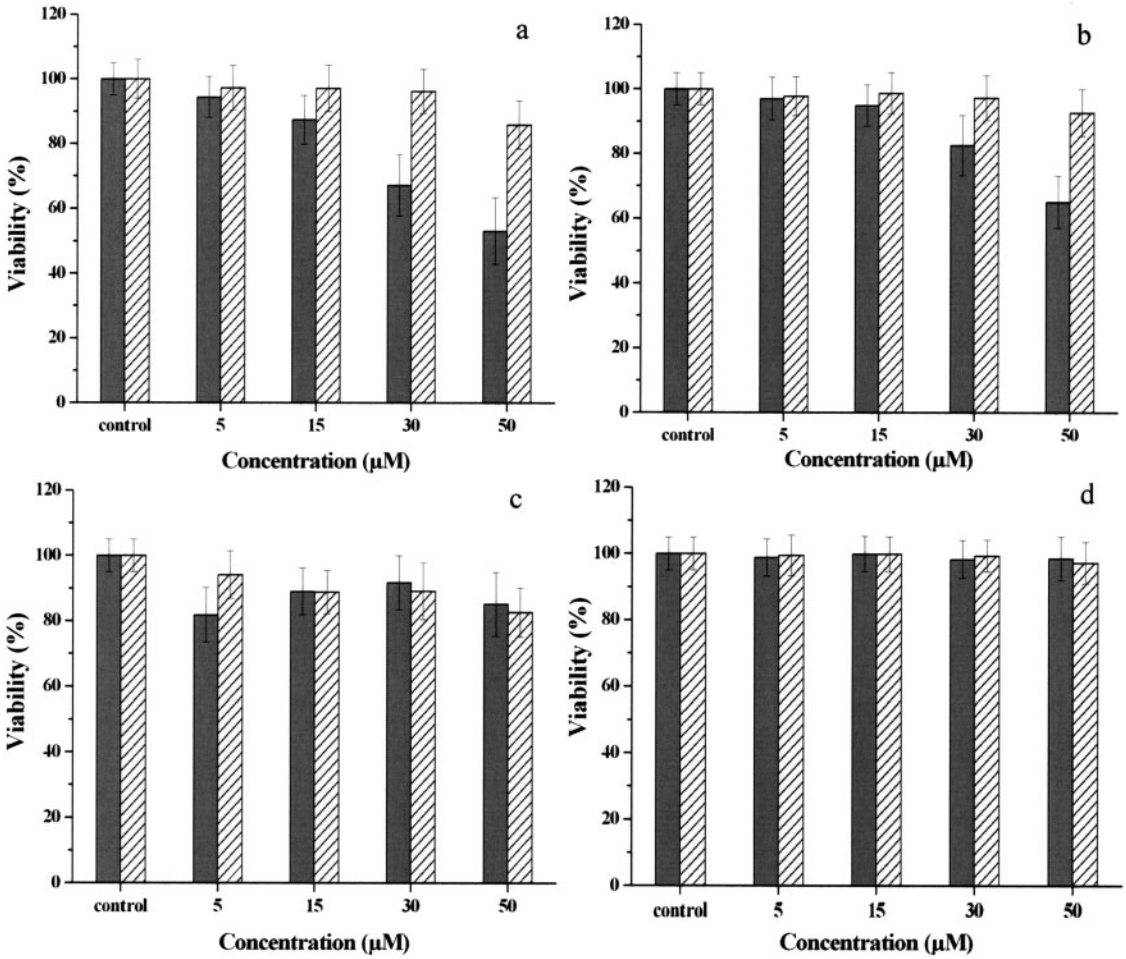

FIG. 4. **Cytotoxic effect of EL amyloid structures measured by EtBr assay.** The cell viability of primary neuronal cells (*a*), primary fibroblasts (*b*), and IMR-32 cells (*c*) were measured in the presence of EL-soluble amyloid oligomers incubated at pH 4.5 (*black bars*) and pH 2.0 (*striped bars*). EL protofilaments formed after 12 days of incubation at pH 4.5 do not affect the viability of primary neuronal cells (*d*). Each data set represents a mean value of three experiments with statistical significance of $p \leq 0.05$.

ferring to the culture medium, the distributions of oligomeric species in both the pH 4.5 and 2.0 samples remained identical to those shown in Fig. 3. After 48 h of incubation in the culture medium, the positions of all of the main peaks in the oligomeric distributions did not change compared with those shown in Fig. 3; however, large amorphous aggregates were observed in the same samples. Similarly, amorphous aggregation was also prompted in the sample of monomeric EL during the same length of incubation in the serum-free culture medium; however, these aggregates were found to be nontoxic.

The AFM imaging of EL oligomers was also performed after 48 h of incubation with IMR-32 cells in the serum-free culture medium at 37 °C. The distinct oligomers and annular protofibrils were monitored in cell supernatants, and their dimensions were estimated using cross-sectional analysis. They displayed the same morphological characteristics as the amyloid structures freshly added to the cells. This confirmed that, once formed, EL amyloid structures remain stable under the conditions of the cytotoxicity assays presented below. Furthermore, the test cells did not affect the morphology of EL amyloid structures.

Cell Viability Measured by EtBr Assay—The effect of amyloid structures on viability of three types of cells, primary neuronal cells, primary fibroblasts, and the neuroblastoma cell line IMR-32, was examined. The cells were subjected to EtBr staining after incubation in the presence of increasing concentrations of amyloid aggregates; the results are presented in Fig. 4. In the control measurements (Fig. 4), there was no difference in cell viability upon the addition of equivalent aliquots of incubation buffer or monomeric EL. The soluble amyloid oligomers induced cell death in a concentration-dependent manner in all cells examined. The effect caused by the oligomers formed at pH 4.5 was more pronounced than the effect from the oligomers assembled at pH 2.0. The primary neuronal cells were most sensitive to treatment with soluble amyloid oligomers; cell death reached 48% at a 50 μM final concentration of EL amyloid produced at pH 4.5 compared with 38% for primary fibroblasts and 12% for IMR-32 cells (Fig. 4, *a*–*c*). However, in all three cell types, the percentage of dead cells did not exceed 10–15% in the presence of the highest concentration (50 μM) of EL amyloid produced at pH 2.0 (Fig. 4, *a*–*c*). By contrast, the fibrillar samples incubated both at pH 4.5 and 2.0 for 12–24 days were not toxic; within the same protein concentration range, they did not induce death in the most sensitive primary neuronal cell culture (Fig. 4*d*).

Cell Viability Measured by MTT Reduction and DNA Fragmentation—The effect of amyloid structures on the oxidative metabolism of IMR-32 cells was evaluated by MTT assay, in which the metabolic activity of the cells was assessed by their ability to cleave MTT to a water-insoluble formazan (28). The cell viability decreased with increasing protein concentrations reaching a maximum toxic effect of ~30 and ~15% in the presence of 64 μM EL amyloid aggregates formed at pH 4.5 and 2.0, respectively (Fig. 5). EL amyloid protofilaments formed both at pH 4.5 and 2.0 (Fig. 2*b*) did affect the cleavage of MTT by IMR-32 cells.

Downloaded from http://www.jbc.org/ by guest on January 16, 2014

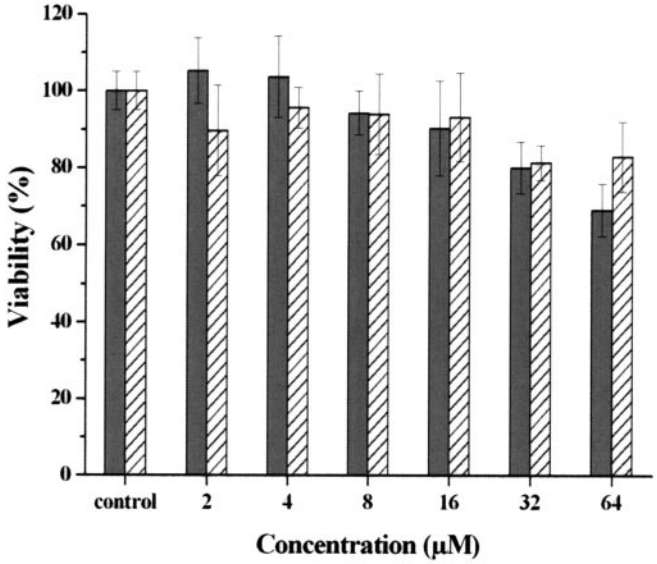

FIG. 5. **The viability of IMR-32 cells in the presence of EL-soluble amyloid oligomers evaluated by MTT reduction assay.** EL-soluble amyloid oligomers were incubated at pH 4.5 (*black bars*) and pH 2.0 (*striped bars*). Each data set represents a mean value of six measurements. $p \leq 0.05$.

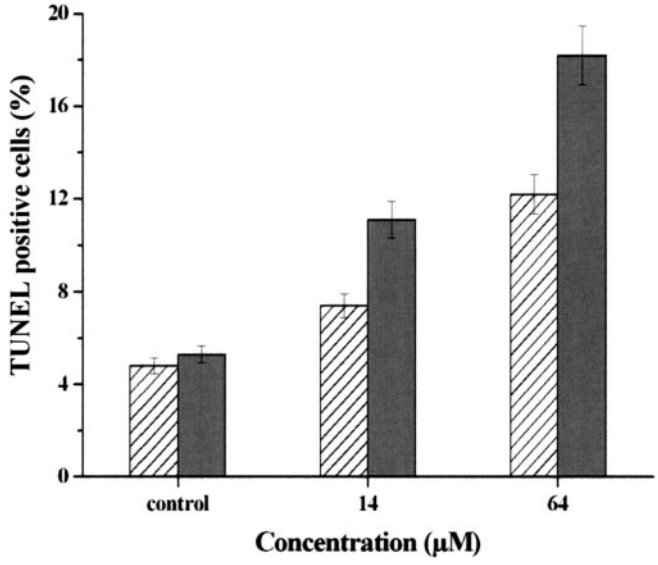

FIG. 6. **Fractionation of DNA in IMR-32 cells induced by EL-soluble amyloid oligomers and measured by the TUNEL method.** EL oligomers were incubated at pH 4.5 (*black bars*) and pH 2.0 (*striped bars*). $p \leq 0.05$.

TUNEL assay was used as a marker for determining apoptotic cell death (4). The experiments revealed a concentration-dependent effect of EL amyloid aggregates on DNA fragmentation in IMR-32 cells (Fig. 6). However, the effect was somewhat higher after the addition of 64 μM EL incubated at pH 4.5 (18%) than in the presence of the similar EL aliquot aggregated at pH 2.0 (12%).

DISCUSSION

Protein aggregation generates a very broad range of structures including oligomers, protofibrils, and fibrils. Monomeric EL and higher order oligomers were visualized and characterized by AFM (see "Experimental Procedures"). Although EL monomers are apparently prevalent in solution, we have found that tetramers were formed as the first distinct oligomers (Table I). Size distributions of oligomers depend on pH of protein incubation. In the pH 2.0 sample, the largest oligomers that were found were octamers, whereas in the pH 4.5 EL solutions, we detected both octamers and larger species corresponding to 20–25-mer in size (Table I). Here we demonstrated that EL monomers and fibrillar species are not toxic; however, the solutions containing soluble amyloid oligomers induce cell damage and death. Moreover, the toxicity significantly increases with the growing size of oligomers. Even a relatively small increase of fractions of larger oligomers (octa- and 20-mer) in the pH 4.5 sample produces a dramatic cytotoxic effect on the primary cells (Fig. 4) compared with the pH 2.0 sample.

Similarly, α-lactalbumin, a protein which is structurally homologous to EL, forms multimeric protein-lipid complexes that induce apoptosis after intratumoral administration in the brain (10). The cytotoxic effect of oligomers of amyloid β peptide and α-synuclein has been characterized in numerous studies using a wide range of cell types (8, 9, 12, 30). Nonfibrillar species of the SH3 domain or HypF-N were also found to be cytotoxic (11). Our results on cytotoxicity of soluble amyloid oligomers of EL, protein which is abundant in milk and other body fluids, also indicate that toxicity is an intrinsic property of soluble amyloid oligomers.

It is interesting to note that EL can assemble into amyloid rings in a calcium-dependent manner (18). However, under the conditions of cytotoxicity assay, calcium ions are present in the culture medium, and the proportion of rings varies in both samples incubated at pH 2.0 and 4.5. We have not discovered any correlation between the degree of cytotoxicity and the number of annular structures observed in both samples. Rather, the cytotoxic effect clearly depends on the presence of larger oligomers in EL samples (Figs. 4–6). Fig. 2 shows that the rings exhibit a clearly segmented structure, and the molecular dimensions of the segments are similar to the parameters of individual oligomers present in solution, which suggests that the rings can be formed from round-shaped oligomers. A similar morphology was observed in the amyloid rings of the *de novo* designed protein albebetin, which also demonstrate a well defined segmentation and are assembled from oligomers (31).

In the present study, we compared the cytotoxicity induced by EL on three cell types. The primary cells and primary neuronal cells, in particular, are the most susceptible to the toxic effect of EL oligomers. Similarly, selective degradation of human central nervous system neuronal cells *in vitro* induced by soluble oligomeric amyloid β peptide has been reported previously (32). Three methods measuring cell viability in the presence of EL amyloid, including EtBr staining of the damaged cells, MTT reduction assay measuring cell metabolic activity, and the TUNEL method evaluating DNA degradation, gave consistent results, indicating that the oligomers induce cell death in a concentration-dependent manner. The results from TUNEL assay, aimed at labeling apoptotic cells, indicated that the oligomers formed at pH 4.5 are more toxic to the neuroblastoma cell line than the pH 2.0 sample. It is interesting to note that the diameter of the EL tetramer calculated from AFM volume measurements and using spherical cap approximation (21) equals ~3 nm, which is close to the cytoplasmic membrane thickness of 3–8 nm (33). We hypothesize that larger amyloid-prone species can induce destruction of cytoplasmic membranes through insertion into a lipid bilayer similar to the pore-like activity *in vitro* of α-synuclein annular protofibrils (30).

Ubiquitous protein, such as lysozyme, which is present under a variety of conditions *in vivo*, can be prompted spontaneously to aggregate into multimeric species in the body. As amyloidogenicity is viewed as a generic property of the polypeptide chain (1), a variety of proteins can enter the amyloid pathway. Recently, we have shown that, in the early stages of

Downloaded from http://www.jbc.org/ by guest on January 16, 2014

dementia, the immune system removes aggregated species of both amyloid β peptide and lysozyme from the serum of Alzheimer's patients, among which the former is related and the latter is not directly involved in the disease (34). Immune response is considered as a clearance pathway able to eliminate aggregating proteins causing amyloid development (34). This demonstrates that soluble oligomeric species of amyloid-forming proteins, rather than mature fibrils, can be considered as a primary therapeutic target and diagnostic marker in protein aggregation diseases.

Acknowledgments—We thank Wim Noppe for providing equine lysozyme, Andrey Shchukarev for latex samples, Alexander Talyzin for carbon nanotubes, and the Innovita Research Foundation for primary cell cultures and acknowledge the grant for travel from the Visby Programme of the Swedish Institute. The atomic force microscope was purchased with the grant generously provided by the Kempe Foundation.

REFERENCES

1. Dobson, C. M. (2003) *Nature* **426,** 884–890
2. Hammarstrom, P., Schneider, F., and Kelly, J. W. (2001) *Science* **293,** 2459–2462
3. Goldberg, M. S., and Lansbury, P. T., Jr. (2000) *Nat. Cell Biol.* **2,** 115–119
4. Andersson, K., Olofsson, A., Nielsen, E. H., Svehag, S. E., and Lundgren, E. (2002)*) Biochem. Biophys. Res. Commun.* **294,** 309–314
5. Pepys, M. B., Hawkins, P. N., Booth, D. R., Vigushin, D. M., Tennent, G. A., Soutar, A. K., Totty, N., Nguyen, O., Blake, C. C., Terry, C. J., Feest, G., Zalin, A. M., and Hsuan J. J. (1993) *Nature* **362,** 553–557
6. Harrison, R. F., Hawkins, P. N., Roche, W. R., MacMahon, R. F., Hubscher, S. G., and Buckels, J. A. (1996) *Gut* **38,** 151–152
7. Lee, K. W., Lee, S. H., Kim, H., Song, J. S., Yang, S. D., Paik, S. G., and Han, P. L. (2004) *J. Neurosci. Res.* **76,** 572–580
8. Gong, Y., Chang, L., Viola, K. L., Lacor, N. P., Lambert, M. P., Finch, C. E., Krafft, G. A., and Klein, W. L. (2003) *Proc. Natl. Acad. Sci. U. S. A.* **100,** 10417–10422
9. Chromy, B. A., Nowak, R. J., Lambert, M. P., Viola, K. L., Chang, L., Velasco, P. T., Jones, B. W., Fernandez, S. J., Lacor, P. N., Horowitz, P., Finch, C. E., Krafft, G. A., and Klein, W. L. (2003) *Biochemistry* **42,** 12749–12756
10. Svensson, M., Hakansson, A., Mossberg, A. K., Linse, S., and Svanborg, C. (2000) *Proc. Natl. Acad. Sci. U. S. A.* **97,** 4221–4226
11. Bucciantini, M., Giannoni, E., Chiti, F., Baroni, F., Formigli, L., Zurdo, J., Taddei, N., Ramponi, G., Dobson, C. M., and Stefani, M. (2002) *Nature* **416,** 507–511
12. Hoshi, M., Sato, M., Matsumoto, S., Noguchi, A., Yasutake, K., Yoshida, N., and Sato, K. (2003) *Proc. Natl. Acad. Sci. U. S. A.* **100,** 6370–6375
13. Morozova-Roche, L. A., Jones, J. A., Noppe, W., and Dobson, C. M. (1999) *J. Mol. Biol.* **289,** 1055–1073
14. Morozova-Roche, L. A., Arico-Muendel, C. C., Haynie, D. T., Emelyanenko, V. I., Van Dael, H., and Dobson, C. M. (1997) *J. Mol. Biol.* **268,** 903–921
15. Morozova, L. A., Haynie, D. T., Arico-Muendel, C., Van Dael, H., and Dobson, C. M. (1995) *Nat. Struct. Biol.* **2,** 871–875
16. Morozova-Roche, L. A., Zurdo, J., Spencer, A., Noppe, W., Receveur, V., Archer, D. B., Joniau, M., and Dobson, C. M. (2000) *J. Struct. Biol.* **130,** 339–351
17. Goers, J., Permyakov, S. E., Permyakov, E. A., Uversky, V. N., and Fink, A. L. (2002) *Biochemistry* **41,** 12546–12551
18. Malisauskas, M., Zamotin, V., Jass, J., Noppe, W., Dobson, C. M., and Morozova-Roche, L. A. (2003) *J. Mol. Biol.* **330,** 879–890
19. Noppe, W., Hanssens, I., and De Cuyper, M. (1996) *J. Chromatogr. A* **719,** 327–331
20. Klunk, W. E., Pettegrew, J. W., and Abraham, D. J. (1989) *J. Histochem. Cytochem.* **37,** 1273–1281
21. Schneider, S. W., Larmer, J., Henderson, R. M., and Oberleithner, H. (1998) *Pflgers Arch.* **435,** 362–367
22. Geisse, N. A., Wasle, B., Saslowsky, D. E., Henderson, R. M., and Edwardson, J. M. (2002) *J. Membr. Biol.* **189,** 83–92
23. Dorman, D. C., Bolon, B., and Morgan, K. T. (1993) *Toxicol. Appl. Pharmacol.* **122,** 265–272
24. Piras, G., El Kharroubi, A., Kozlov, S., Escalante-Alcalde, D., Hernandez, L., Copeland, N. G., Gilbert, D. J., Jenkins, N. A., and Stewart, C. (2000) *Mol. Cell. Biol.* **20,** 3308–3315
25. Watjen, W., Haase, H., Biagioli, M., and Beyersmann, D. (2002) *Environ. Health Perspect.* **110,** 865–867
26. Roher, A. E., Chaney, M. O., Kuo, Y. M., Webster, S. D., Stine, W. B., Haverkamp, L. J., Woods, A. S., Cotter, R. J., Tuohy, J. M., Krafft, G. A., Bonnell, B. S., and Emmerling, M. R. (1996) *J. Biol. Chem.* **271,** 20631–20635
27. Arata, T., Oyama, Y., Tabaru, K., Satoh, M., Hayashi, H., Ishida, S., and Okano, Y. (2002) *Environ. Toxicol.* **17,** 472–477
28. Datki, Z., Juhasz, A., Galfi, M., Soos, K., Papp, R., Zadori, D., and Penke, B. (2003) *Brain Res. Bull.* **62,** 223–229
29. Harper, J. D., and Lansbury, P. T., Jr. (1997) *Annu. Rev. Biochem.* **66,** 385–407
30. Ding, T. T., Lee, S. J., Rochet, J. C., and Lansbury, P. T., Jr. (2002) *Biochemistry* **41,** 10209–10217
31. Morozova-Roche, L. A., Zamotin, V. V., Malisauskas, M., Öhman, A., Chertkova, R., Lavrikova, M. A., Kostanyan, I. A., Dolgikh, D. A., and Kirpichnikov, M. P. (2004) *Biochemistry*, **43,** 9610–9619.
32. Kim, H. J., Chae, S. C., Lee, D. K., Chromy, B., Lee, S. C., Park, Y. C., Klein, W. L., Krafft, G. A., and Hong, S. T. (2003) *FASEB J.* **17,** 118–120
33. Alberts, B., Bray, D., Lewis, J., Raff, R., Roberts, K., and Watson, J. D. (1994) *Molecular Biology of the Cell*, 3rd Ed., Garland Publishing, New York
34. Gruden, M. A., Davudova, T. B., Malisauskas, M., Zamotin, V. V., Sewell, R. D. E., Voskresenskaya, N. I., Kostanyan, I. A., Sherstneva, V. V., and Morozova-Roche, L. A. (2004) *Dement. Geriatr. Cogn. Disord.* **18,** 165–171

Downloaded from http://www.jbc.org/ by guest on January 16, 2014